Detailed mechanism of the CH2I + O2 reaction: Yield and self-reaction of the simplest Criegee intermediate CH2OO

Wei-Lun Ting, Chun-Hung Chang, Yu-Fang Lee, Hiroyuki Matsui, Yuan-Pern Lee, and Jim Jr-Min Lin

Citation: The Journal of Chemical Physics **141**, 104308 (2014); doi: 10.1063/1.4894405
View online: http://dx.doi.org/10.1063/1.4894405
View Table of Contents: http://scitation.aip.org/content/aip/journal/jcp/141/10?ver=pdfcov
Published by the AIP Publishing

Detailed mechanism of the $CH_2I + O_2$ reaction: Yield and self-reaction of the simplest Criegee intermediate CH_2OO

Wei-Lun Ting,[1] Chun-Hung Chang,[1] Yu-Fang Lee,[2] Hiroyuki Matsui,[2] Yuan-Pern Lee,[1,2,a)] and Jim Jr-Min Lin[1,2,3,a)]

[1]*Institute of Atomic and Molecular Sciences, Academia Sinica, Taipei 10617, Taiwan*
[2]*Department of Applied Chemistry and Institute of Molecular Science, National Chiao Tung University, 1001, Ta-Hsueh Road, Hsinchu 30010, Taiwan*
[3]*Department of Chemistry, National Taiwan University, Taipei, Taiwan*

(Received 29 May 2014; accepted 20 August 2014; published online 9 September 2014)

The application of a new reaction scheme using $CH_2I + O_2$ to generate the simplest Criegee intermediate, CH_2OO, has stimulated lively research; the Criegee intermediates are extremely important in atmospheric chemistry. The detailed mechanism of $CH_2I + O_2$ is hence important in understanding kinetics involving CH_2OO. We employed ultraviolet absorption to probe simultaneously CH_2I_2, CH_2OO, CH_2I, and IO in the reaction system of $CH_2I + O_2$ upon photolysis at 248 nm of a flowing mixture of CH_2I_2, O_2, and N_2 (or SF_6) in the pressure range 7.6–779 Torr to investigate the reaction kinetics. With a detailed mechanism to model the observed temporal profiles of CH_2I, CH_2OO, and IO, we found that various channels of the reaction $CH_2I + O_2$ and $CH_2OO + I$ play important roles; an additional decomposition channel of $CH_2I + O_2$ to form products other than CH_2OO or ICH_2OO becomes important at pressure less than 60 Torr. The pressure dependence of the derived rate coefficients of various channels of reactions of $CH_2I + O_2$ and $CH_2OO + I$ has been determined. We derived a rate coefficient also for the self-reaction of CH_2OO as $k = (8 \pm 4) \times 10^{-11}$ cm^3 molecule^{-1} s^{-1} at 295 K. The yield of CH_2OO from $CH_2I + O_2$ was found to have a pressure dependence on N_2 and O_2 smaller than in previous reports; for air under 1 atm, the yield of ~30% is about twice of previous estimates. © *2014 AIP Publishing LLC*. [http://dx.doi.org/10.1063/1.4894405]

I. INTRODUCTION

The reactions of O_3 with alkenes are extremely important because they are responsible for the removal of both O_3 and unsaturated hydrocarbons, and for the production of OH and organic aerosols in the troposphere.[1–3] The current model indicates that cycloaddition of O_3 to the C=C double bond of unsaturated hydrocarbons forms a primary cyclic ozonide, which rapidly cleaves its C–C and O–O bonds to form a carbonyl molecule and a carbonyl oxide that is commonly referred to as the Criegee intermediate.[4–9] Previous understanding of the mechanism of these reactions was based on indirect laboratory observations of stable end products because the Criegee intermediates have eluded direct detection until recently.[10,11]

The recent applications of a new reaction scheme using $CH_2I + O_2$ to generate the simplest Criegee intermediate, CH_2OO, have stimulated lively research. Using this reaction scheme, CH_2OO has been detected with photoionization mass spectrometry,[12] ultraviolet (UV) depletion,[13] UV absorption,[14,15] infrared (IR) absorption,[16] and microwave spectroscopy.[17,18] With the use of some of these detection methods, the kinetics of reactions of CH_2OO with various compounds have been investigated experimentally.[12,19–22] Even though the reaction of $CH_2I + O_2$ has been investigated extensively,[23–31] a detailed mechanism of this reaction still needs to be established. The total rate coefficient for the reaction of $CH_2I + O_2$ was reported to be (1.28–1.82) $\times 10^{-12}$ cm^3 molecule^{-1} s^{-1},[14,24,26,29,31] but the branching of various formation channels was not clearly characterized. The proposed mechanisms in the earlier studies were incomplete because only product channels for the formation of ICH_2OO and $H_2CO + IO$, not CH_2OO, were considered. The mechanisms employed in more recent reports include the formation of CH_2OO but not the rapid self-reaction of CH_2OO and various channels of the reaction of $CH_2OO + I$; these reactions become important in some laboratory experiments involving large concentrations of CH_2OO and I. A more detailed understanding of the $CH_2I + O_2$ system covering experimental conditions over a wide range is thus desirable.

Using transient IR absorption to probe directly the decay of CH_2OO, we found that the self-reaction $CH_2OO + CH_2OO$ was extremely rapid,[21] and estimated the rate coefficient of this self-reaction to be $(4 \pm 2) \times 10^{-10}$ cm^3 molecule^{-1} s^{-1} at 343 K. According to quantum-chemical calculations, this reaction is rapid because a cyclic dimeric intermediate is formed with large exothermicity (~375 kJ mol^{-1}) before further decomposition to 2 $H_2CO + O_2$ ($^1\Sigma_g$). The formation of this dimer, with the terminal O atom of one CH_2OO bound to the C atom of the other CH_2OO, reflects a unique property of the zwitterionic character of CH_2OO in which the

a)Authors to whom correspondence should be addressed. Electronic addresses: yplee@mail.nctu.edu.tw and jimlin@gate.sinica.edu.tw

terminal oxygen atom is partially negatively charged whereas the other oxygen atom and the C atom are partially positively charged. While we were preparing this manuscript, a recent report by Buras *et al.* indicated that the rate coefficient of this self-reaction of CH_2OO, $(6.0 \pm 2.1) \times 10^{-11}$ cm^3 $molecule^{-1}$ s^{-1} at 297 K, is much smaller than our previous estimate at 343 K;[32] the kinetics were investigated with probes of CH_2OO at 375 nm and I atom at 1315 nm.

We have performed new experiments to probe simultaneously the UV absorption of CH_2I_2, CH_2OO, IO, and CH_2I upon photolysis at 248 nm of a flowing mixture of CH_2I_2, O_2, and N_2 in the pressure range 7.6–779 Torr. The temporal profiles of CH_2OO and IO were analyzed simultaneously with a detailed reaction mechanism and the pressure dependence of the yield of CH_2OO and rate coefficients of various channels of $CH_2I + O_2$ and $CH_2OO + I$ has been characterized. The rate coefficient of $CH_2OO + CH_2OO$ at 295 K was determined to be $(8 \pm 4) \times 10^{-11}$ cm^3 $molecule^{-1}$ s^{-1}.

II. EXPERIMENTS

The photolysis cell with transient UV absorption detection has been described previously;[33,34] only relevant details are given here. The Criegee intermediate CH_2OO was produced from the reaction of CH_2I with O_2; CH_2I was prepared by photodissociation of CH_2I_2 at 248 nm.

The photolysis laser beam and the probe light (both diameter 1.8 cm) overlapped collinearly in the reaction cell (length 75 cm, inner diameter 2.0 cm), as shown in Fig. 1. The photolysis laser beam at 248 nm from an excimer laser (Coherent, CompExPro 205F, KrF, ~50 mJ, 1 Hz) was introduced into the cell by reflection from an ultra-steep long-pass edge filter (Semrock LP02-257RU-25), which also limited the probe wavelength to be greater than 260 nm. The output of a high-brightness broadband light source (Energetiq, EQ-99) was collimated with a parabolic mirror ($f = 50.8$ mm) before entering the reaction cell. Another parabolic mirror ($f = 101.6$ mm) served to focus the light onto the slit of a spectrometer (Andor SR303i) equipped with an intensified charge-coupled detector (iCCD, Andor iStar, DH320T-18F-E3). The resolution of the spectrometer was ~1.5 nm. The wavelength was calibrated with the emission spectrum of a low-pressure mercury lamp, with typical errors smaller than 0.5 nm.

The transient absorption spectra were recorded with the array detector at varied delays after photolysis. The delay (duration of reaction) was defined as the interval from the photolysis laser pulse to the center of the detector gate (width = 1 μs). The reference spectrum was taken at 1 or 5 μs before the photolysis laser pulse. The integration interval at each delay was 1 μs; the delay was scanned automatically after each photolysis pulse with a computer program written in Andor Basic. The spectrum at a specific delay was typically averaged 60–200 times to achieve an adequate ratio of signal to noise.

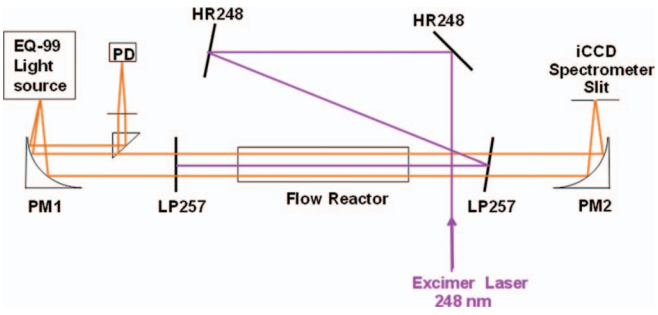

FIG. 1. Schematic experimental setup (not to scale). PM: parabolic mirror; HR248: highly reflective mirror at 248 nm; LP257: long-pass filter at 257 nm; PD: photodiode; and iCCD: image-intensified CCD camera.

A small fraction of CH_2 might be produced through the photolysis of CH_2I. We have tested the transient absorption spectra with laser pulse energies varied from 30 to 100 mJ $pulse^{-1}$. A small decrease (2%–4%) in the yield of CH_2I was observed at laser energy greater than 100 mJ $pulse^{-1}$, but an insignificant difference in the deduced spectrum of CH_2OO was found.

Liquid CH_2I_2 was slightly heated to 305 K to ensure saturation of its vapor pressure and the CH_2I_2 vapor was carried with a flow of N_2 or O_2. The mixing ratios of the reagent gases (CH_2I_2, N_2, O_2, SF_6) were controlled with mass flow controllers (Brooks Instruments, 5850E). These gases were mixed in a Teflon tube before entering the reaction cell. A small stream (1%–2% of the total mass flow) of the N_2/O_2 mixture gas (with the same ratio as the reagent gas) was introduced to purge both windows of the cell to prevent undesired photochemistry at the window surfaces. This purging also decreased the effective length of the sample from 75 to 72 cm, which was calibrated with the absorbance of CH_2I_2/N_2 gas of a known mixing ratio.

The linear flow velocity in the reaction cell was adjusted to be greater than 0.8 m s^{-1} to allow refreshment of the sample gas between the photolysis laser pulses at a repetition rate of 1 Hz. The temperature of the reaction cell was 295 ± 1.5 K. The number density of CH_2I_2 was determined from its absorption spectrum. The number densities of O_2 and N_2 were deduced with the ideal gas law from the measured cell pressure and their mass flow rates.

III. RESULTS

A. Determination of Δ[CH_2I_2], [CH_2I], [CH_2OO], and [IO]

A representative transient difference UV absorption spectrum recorded 9 μs after photolysis of a flowing mixture of $CH_2I_2/O_2/N_2$ (0.044/10.4/90.7) at 101.1 Torr is shown in Fig. 2. The spectrum was deconvoluted to spectra of CH_2I_2 (negative due to depletion), IO, CH_2OO, and CH_2I, as is discernible from the small residual after subtracting corresponding spectra of these four species. The absorption spectra of CH_2OO and IO have characteristic progressions, whereas those of CH_2I_2 and CH_2I are broad but different in shape. On minimizing the residual between the simulated and experimental spectra in the region 265–480 nm with a least-squares fitting, the number densities of CH_2OO, IO, and CH_2I, and the decrease of that of CH_2I_2 after photolysis, were deduced according to the cross sections of these species (CH_2I_2 and IO,[35] CH_2I,[23] and CH_2OO).[15] The uncertainties in concentration measurements of CH_2OO, IO, CH_2I, and CH_2I_2 from deconvolution were estimated to be ~5%, 5%, 10%, and 5%,

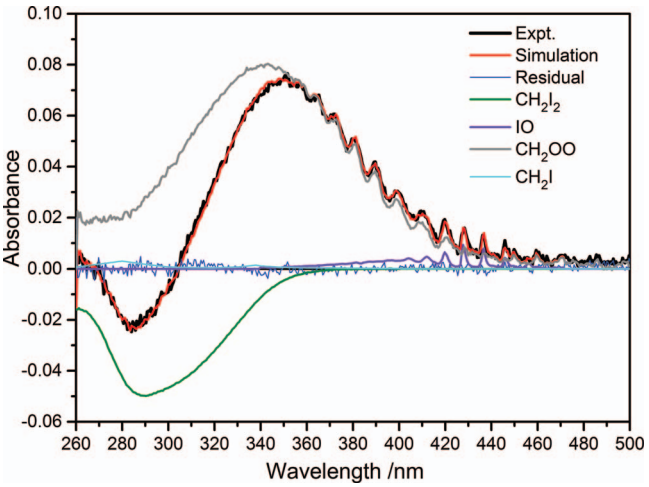

FIG. 2. Comparison of experimental and simulated transient absorption spectra. The total simulation consists of absorbance of CH_2I_2 (depletion), IO, CH_2OO, and CH_2I. In this example (experiment no. 50), $-\Delta[CH_2I_2] = 1.82 \times 10^{14}$, $[IO] = 6.56 \times 10^{12}$, $[CH_2OO] = 9.01 \times 10^{13}$, $[CH_2I] = 4.98 \times 10^{12}$ molecule cm^{-3}. Other experimental conditions are P = 101 Torr, $P_{O_2} = 10.4$ Torr, $P_{N_2} = 90.7$ Torr, $P_{CH_2I_2} = 43.7$ mTorr, and delay time = 9 μs.

respectively; errors throughout this report are 1σ in fitting unless stated otherwise. In this case the uncertainties in cross sections are not included in the error estimates.

At higher pressure and at a later period of reaction, the product ICH_2OO becomes important. The reported UV cross section of ICH_2OO, with a maximum value $\geq 1.7 \times 10^{-18}$ cm^2 $molecule^{-1}$ (Ref. 27) or 2.5×10^{-18} cm^2 $molecule^{-1}$ near 330 nm,[23] is much smaller than that of CH_2OO that has a maximal value 1.2×10^{-17} cm^2 $molecule^{-1}$ at 340 nm.[15] At 760 Torr, the concentration of ICH_2OO might become twice that of CH_2OO; consequently, using the reported cross section of ICH_2OO, ICH_2OO might contribute up to ~30% of observed UV absorption near 340 nm. However, according to theoretical calculations, ICH_2OO is not the main carrier of the previously observed spectrum in the region 275–450 nm;[36] absorption of CH_2OO might have some contribution. To clarify this issue, we utilized the characteristic oscillatory pattern in the region 352–404 nm, likely due to a vibronic progression of CH_2OO, to show that the presence of ICH_2OO at high pressure affects little our determination of CH_2OO concentrations from observed UV spectra, as discussed in Sec. I and demonstrated in Fig. S1 of the supplementary material.[37]

Because the rate coefficient of the self-reaction of CH_2OO requires accurate measurements of $[CH_2OO]$, the accuracy of the UV cross section of CH_2OO is important. As compared in our previous paper,[15] for CH_2OO near 295 K, the UV absorption spectrum reported by Sheps[14] agrees with our spectrum showing similar vibronic structures on the long-wavelength side, but decreases in absorbance much more rapidly than ours on the structureless short-wavelength side. More importantly, the cross sections reported by Sheps[14] were approximately 3.3 times ours. We think that our measurements are more reliable for the following reasons: (1) Our technique has mass selectivity and employs a depletion method to compare with a known reference molecule. This method was proved reliable in the measurements of cross sections of ClOOCl.[38] (2) We utilized both the SO_2 scavenging reaction and the self-reaction of CH_2OO to extract the CH_2OO spectrum and obtained consistent results with signal-to-noise ratios superior to other reports. (3) If we used the cross section of Sheps, not only the transient absorption spectra could not be deconvoluted satisfactorily, but also the yield of CH_2OO from $CH_2I + O_2$ at low pressure would become ~0.25, much smaller than the values 0.87–1.0 reported by Huang *et al.*[30] and 0.67–1.0 reported by Stone *et al.*[31] With the cross section determined by us, the yield 0.72–0.78 agrees with those in previous reports. (4) Buras *et al.* recently reported cross sections of CH_2OO at 375 nm to be $(7\pm^{7}_{3.5}) \times 10^{-18}$ cm^2 $molecule^{-1}$ (Ref. 39) and $(6.2 \pm 2.2) \times 10^{-18}$ cm^2 $molecule^{-1}$,[32] in satisfactory agreement with our value of $(7.6 \pm 1.1) \times 10^{-18}$ cm^2 $molecule^{-1}$ with the uncertainty limits overlapping with each other.

B. Temporal profiles of CH_2OO and IO in experiments with N_2 and O_2

A summary of experimental conditions and fitted rate coefficients of some representative experiments is presented in Table I; a complete list of a total of 64 experiments is available in Table SI of the supplementary material.[37]

Representative temporal profiles of CH_2I, CH_2OO, and IO recorded upon photolysis of a flowing mixture of CH_2I_2 (24.3 or 24.5 mTorr), O_2 (both 10.5 Torr), and N_2 (92.7 or 90.4 Torr) in two experiments (nos. 60 and 63 in Table I) near 100 Torr and 295 K with small $[CH_2OO]_0$ are shown in Fig. 3. The decrease in concentration of CH_2I_2 upon laser irradiation, hence $[CH_2I]_0$, was $-\Delta[CH_2I_2] = [CH_2I]_0 \cong 1.17$ mTorr (3.8×10^{13} molecule cm^{-3}). The rapid increase of CH_2OO and decay of CH_2I were due to the reaction of $CH_2I + O_2$. After approximately 8 μs, CH_2OO began to decay and the concentration of IO gradually increased. In this figure (and all others showing experimental temporal profiles) we also show the simulated temporal profiles of CH_2I, CH_2OO, IO, ICH_2OO, H_2CO, and I according to the proposed mechanism, as discussed in Sec. IV A.

For comparison, Fig. 4 shows results of two experiments (nos. 49 and 52 in Table I) under similar conditions except for increased $[CH_2OO]_0$. The decrease in concentration of CH_2I_2 upon laser irradiation, hence $[CH_2I]_0$, was $-\Delta[CH_2I_2] = [CH_2I]_0 \cong 3.54$ mTorr (1.16×10^{14} molecule cm^{-3}). In this example, $[CH_2OO]$ decreased more rapidly than in Fig. 3, indicating the second-order nature of the decay of CH_2OO. Similarly, [IO] increased more rapidly than in Fig. 3, indicating that some IO was produced from subsequent reactions of CH_2OO.

The temporal profile of CH_2I, CH_2OO, and IO recorded upon photolysis of a flowing mixture of CH_2I_2 (42.9 mTorr), O_2 (51.1 Torr), and N_2 (354.4 Torr) in an experiment (no. 2 in Table I) at high pressure (405.5 Torr) and 295 K is shown in Fig. S2 of the supplementary material.[37] In this example, CH_2OO increased rapidly because of larger $[O_2]$ employed and the yield of IO (and ICH_2OO by simulation) relative to CH_2OO was enhanced, indicating that some IO was produced from secondary reactions of ICH_2OO of which the concentration was expected to be enhanced at high pressure.

TABLE I. Representative experimental conditions, fitted rate coefficients, yield y and fraction of survival β of CH_2OO in the $CH_2I + O_2$ system at 295 K.

Expt. no.	P_{Total} (Torr)	P_{O_2} (Torr)	P_{N_2} (Torr)	$P_{CH_2I_2}$ (mTorr)	$-\Delta[CH_2I_2]$ (10^{13})[a]	k_{1a}' (10^{-12})[b]	k_{1b} (10^{-12})[b]	k_{1c} (10^{-12})[b]	k_3 (10^{-12})[b]	y[c]	β[c]
3	779.2	5.3	773.9	42.3	8.3	0.44	1.06	0.00	104	0.30	1.00
4	777.0	53.1	723.9	42.1	8.5	0.42	1.08	0.00	93	0.28	1.00
36	758.0	163.0	595.0	41.6	9.8	0.56	0.94	0.00	65	0.37	1.00
18	606.6	10.3	596.3	41.3	8.8	0.49	1.01	0.00	109	0.33	1.00
14	602.1	10.4	591.7	26.5	5.8	0.49	1.01	0.00	67	0.33	1.00
13	515.4	10.5	504.9	26.3	6.0	0.51	0.99	0.00	72	0.34	1.00
17	497.8	10.0	487.8	40.5	8.8	0.55	0.95	0.00	97	0.37	1.00
2	405.5	51.1	354.4	42.9	9.1	0.60	0.90	0.00	65	0.40	1.00
35	399.3	85.4	313.9	41.0	10.2	0.69	0.81	0.00	71	0.46	1.00
16	305.3	10.3	295.0	41.2	9.0	0.68	0.82	0.00	91	0.46	1.00
12	304.0	10.3	293.7	26.1	6.0	0.69	0.81	0.00	60	0.46	1.00
15	205.5	10.3	195.2	40.8	9.3	0.79	0.71	0.00	83	0.53	1.00
11	200.1	10.2	189.9	26.9	6.4	0.78	0.72	0.00	74	0.52	1.00
49	104.3	10.8	93.5	43.8	11.4	0.96	0.54	0.00	85	0.64	1.00
60	103.2	10.5	92.7	24.3	3.8	0.94	0.56	0.00	72	0.63	1.00
52	101.0	10.4	90.6	44.5	11.8	0.98	0.52	0.00	84	0.65	1.00
63	100.9	10.5	90.4	24.5	3.8	0.96	0.54	0.00	74	0.64	1.00
53	100.9	10.4	90.5	44.6	18.4	0.96	0.54	0.00	85	0.64	1.00
42	100.5	10.7	89.8	14.3	2.1	1.00	0.50	0.00	82	0.67	1.00
66	62.5	10.3	52.2	49.8	7.6	1.07	0.43	0.00	80	0.71	1.00
65	61.6	10.2	51.4	49.3	7.6	1.08	0.42	0.00	85	0.72	1.00
9	41.0	2.3	38.7	32.2	9.8	1.12	0.18	0.21	104	0.74	0.85
6	40.7	2.3	38.4	37.1	9.2	1.13	0.19	0.18	101	0.75	0.86
25	31.2	5.0	26.2	27.6	7.5	1.12	0.15	0.23	107	0.75	0.83
21	30.9	5.4	25.5	26.4	7.1	1.11	0.14	0.25	97	0.74	0.81
64	21.9	11.0	10.9	40.2	6.7	1.17	0.14	0.19	87	0.78	0.86
8	20.3	2.2	18.1	34.7	9.6	1.15	0.08	0.27	91	0.77	0.81
23	11.1	5.8	5.3	26.1	7.8	1.09	0.07	0.33	79	0.73	0.77
19	10.7	5.5	5.2	27.1	7.3	1.16	0.09	0.24	81	0.78	0.83
33	7.9	7.9	0.0	42.1	15.2	1.08	0.03	0.39	59	0.72	0.73
29	7.6	7.6	0.0	41.0	14.4	1.13	0.04	0.33	62	0.76	0.78

[a]In unit of molecule cm^{-3}.
[b]In unit of cm^3 molecule^{-1} s^{-1}.
[c]$y = k_{1a}'/(k_{1a}' + k_{1b} + k_{1c})$; $\beta = k_{1a}'/(k_{1a}' + k_{1c})$.

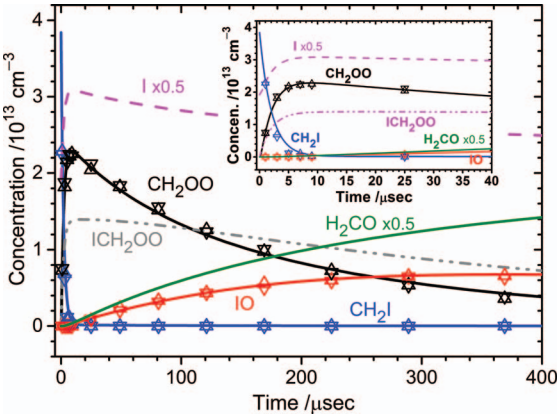

FIG. 3. Temporal profiles of concentrations of IO, CH_2OO, and CH_2I recorded upon photolysis of a flowing mixture of CH_2I_2 (24.3 or 24.5 mTorr), O_2 (both 10.5 Torr), and N_2 (92.7 or 90.4 Torr) at 295 K in two experiments (nos. 60 and 63, symbols Δ and ∇). The decrease of concentration of CH_2I_2 was 1.17 mTorr (3.8×10^{13} molecule cm^{-3}). Concentrations of IO (red), CH_2OO (black), CH_2I (blue), ICH_2OO (gray), I (magenta, scaled by 0.5), and H_2CO (green, scaled by 0.5) simulated with a model described in Sec. IV A are shown as lines. The inset shows a more detailed view in the 0–40 μs region.

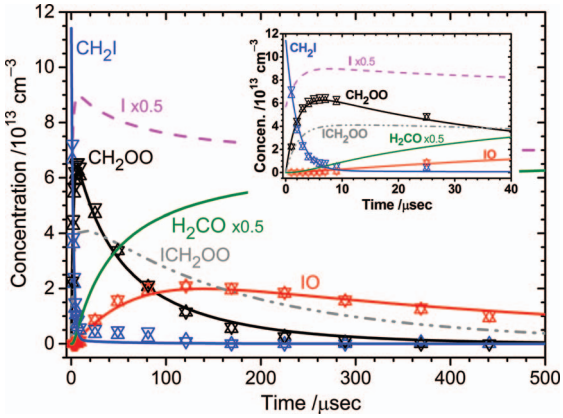

FIG. 4. Temporal profiles of concentrations of IO, CH_2OO, and CH_2I recorded upon photolysis of a flowing mixture of CH_2I_2 (43.8 or 44.5 mTorr), O_2 (10.8 or 10.4 Torr), and N_2 (93.5 or 90.6 Torr) at 295 K in two experiments (nos. 49 and 52, symbols Δ and ∇). The decrease of concentration of CH_2I_2 was 3.53 mTorr (~1.16×10^{14} molecule cm^{-3}). Concentrations of IO (red), CH_2OO (black), CH_2I (blue), ICH_2OO (gray), I (magenta, scaled by 0.5), and H_2CO (green, scaled by 0.5) simulated with a model described in Sec. IV A are shown as lines. The inset shows a more detailed view in the 0–40 μs region.

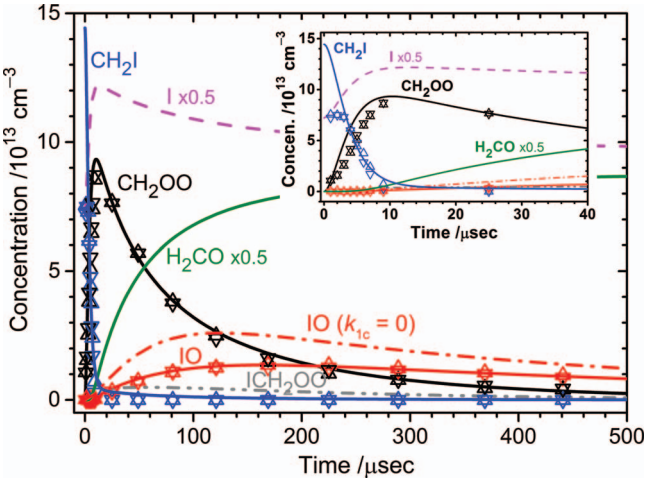

FIG. 5. Temporal profiles of concentrations of IO, CH_2OO, and CH_2I recorded upon photolysis of a flowing mixture of CH_2I_2 (41.0 or 42.1 mTorr) and O_2 (7.6 or 7.9 Torr) at 295 K in two experiments (nos. 29 and 33, symbols Δ and ∇). The decrease of concentration of CH_2I_2 was 4.51 mTorr ($\sim$1.48 $\times$ 10^{14} molecule cm^{-3}). The concentration of IO simulated with the model described in Sec. IV A is shown as dashed-dotted red line. Concentrations of IO (red), CH_2OO (black), CH_2I (blue), ICH_2OO (gray), I (magenta, scaled by 0.5), and H_2CO (green, scaled by 0.5) simulated with a model described in Sec. IV B are shown as lines. The inset shows a more detailed view in the 0–40 μs region.

For experiments at low pressure, representative temporal profiles of CH_2I, CH_2OO, and IO recorded upon photolysis of a flowing mixture of CH_2I_2 (41.0 or 42.1 mTorr) and O_2 (7.6 and 7.9 Torr) in two experiments (nos. 29 and 33 in Table I) at 295 K are shown in Fig. 5. The decrease in concentration of CH_2I_2 upon laser irradiation, hence $[CH_2I]_0$, was $-\Delta[CH_2I_2] = [CH_2I]_0 \cong 4.52$ mTorr (1.48×10^{14} molecule cm^{-3}). The yield of IO (and ICH_2OO by simulation) relative to CH_2OO was diminished as compared with experiments at high pressure. Similar to all experiments with P $\leq$ 20 Torr, the rise of $[CH_2OO]$ was slightly slower than simulated, to be discussed in Sec. IV B. Furthermore, the simulated profile of IO using the same model (Sec. IV A) as that for high pressures (P $\geq$ 100 Torr) is shown in a dashed-dotted line in Fig. 5; it is significantly greater than experimental observation, to be discussed in Sec. IV B.

C. Experiments using SF_6 as a quencher

Five experiments using SF_6 as an efficient quencher in the pressure range 20.0–62.7 Torr at 295 K were performed; the experimental conditions and fitted rate coefficients are presented in Table SII of the supplementary material.[37] A representative temporal profile of CH_2I, CH_2OO, and IO recorded upon photolysis of a flowing mixture of CH_2I_2 (38.3 mTorr), O_2 (5.2 Torr), and SF_6 (15.4 Torr) in an experiment (no. 75 in Table SII) at 20.6 Torr and 295 K is shown in Fig. S3 of the supplementary material.[37] The decrease in concentration of CH_2I_2 upon laser irradiation, hence $[CH_2I]_0$, was $-\Delta[CH_2I_2] = [CH_2I]_0 \cong 3.02$ mTorr (9.9×10^{13} molecule cm^{-3}). Unlike in experiments with N_2 and O_2 below 20 Torr (Fig. 5), the rise of CH_2OO has no delay and can be simulated satisfactorily. Compared with experiments with O_2 and N_2, smaller yields of CH_2OO and IO due to efficient quenching of internally excited ICH_2OO were observed.

IV. DISCUSSION

A. Reaction mechanism and simulation of temporal profiles at P > 60 Torr

To describe the $CH_2I + O_2$ system in detail, we employed the following scheme:

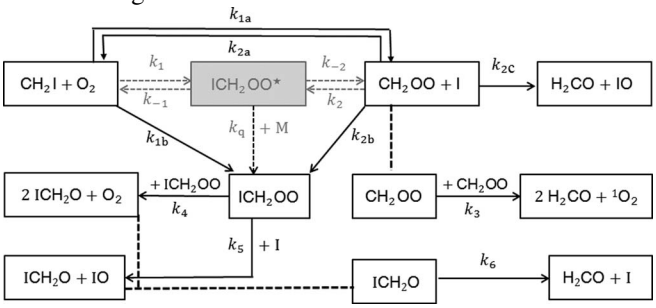

in which ICH_2OO^* represents an energized adduct ICH_2OO initially formed upon reaction of CH_2I with O_2. ICH_2OO^* might decompose to form the original reactants, proceed to form CH_2OO + I (reaction (1a)), or become stabilized to ICH_2OO (reaction (1b)), with branching ratios α_1, α_2, and (1 $-$ α_1 $-$ α_2), respectively. From the steady-state approximation of $[ICH_2OO^*]$, described in detail in the supplementary material,[37] α_1 and α_2 were derived as functions of pressure and detailed rate coefficients indicated in grey in the scheme. The grey part in this scheme was not used explicitly in the kinetic fitting; only the effective reactions (solid parts) were used. Because of the large concentration of I atoms and the great reactivity of CH_2OO, once produced, CH_2OO reacts readily either with I atom (reaction (2)) or with itself (reaction (3)). According to theoretical calculations,[21] the major reactions of CH_2OO with I atom proceed via three channels: attack of the terminal O atom of CH_2OO by the I atom to form H_2CO + IO (reaction (2c)) and attack of the C atom by the I atom to form ICH_2OO^*, followed by formation of CH_2I + O_2 (reaction (2a)) or stabilization to ICH_2OO (reaction (2b)). ICH_2OO further reacts with itself (reaction (4)) or I atoms (reaction (5)) to form ICH_2O which subsequently decomposes to H_2CO + I (reaction (6)).

The mechanism is summarized below:

$$CH_2I + O_2 \rightarrow CH_2OO + I, \qquad k_{1a} = \alpha_2 k_1, \tag{1a}$$

$$CH_2I + O_2 \xrightarrow{M} ICH_2OO, \qquad k_{1b} = (1 - \alpha_1 - \alpha_2)k_1, \tag{1b}$$

$$CH_2OO + I \rightarrow CH_2I + O_2, \qquad k_{2a} = \alpha_1 k_2, \tag{2a}$$

$$CH_2OO + I \xrightarrow{M} ICH_2OO, \qquad k_{2b} = (1 - \alpha_1 - \alpha_2)k_2, \tag{2b}$$

$$CH_2OO + I \rightarrow H_2CO + IO, \qquad k_{2c}, \tag{2c}$$

$$CH_2OO + CH_2OO \rightarrow 2H_2CO + O_2(^1\Delta_g), \qquad k_3, \tag{3}$$

$$ICH_2OO + ICH_2OO \rightarrow 2ICH_2O + O_2 \qquad k_4, \tag{4}$$

$$ICH_2OO + I \rightarrow ICH_2O + IO, \qquad k_5, \tag{5}$$

$$ICH_2O \rightarrow H_2CO + I, \qquad k_6, \tag{6}$$

$$IO + IO \rightarrow \text{products} \qquad k_7 \tag{7}$$

in which $k_4 = 9.0 \times 10^{-11}$ cm^3 molecule^{-1} s^{-1},[27] $k_5 = 3.5 \times 10^{-11}$ cm^3 molecule^{-1} s^{-1}, $k_6 = 1.0 \times 10^5$ s^{-1},[27] and $k_7 = 9.9 \times 10^{-11}$ cm^3 molecule^{-1} s^{-1} were reported.[40]

Even though five rate coefficients are listed for reactions (1) and (2), we had to determine only k_{1a}, k_{1b}, and k_{2c} because $K^{-1} = k_{2a}/k_{1a} = \alpha_1 k_2/\alpha_2 k_1 = \alpha_1 k_{2b}/\alpha_2 k_{1b}$ in which K is the equilibrium constant of reaction (1a). According to calculations with the CCSD(T)//B3LYP/aug-cc-pVTZ-pp method, $\Delta G = 10.4$ kJ mol^{-1} for reaction (1a); hence $K^{-1} = 71$. Once k_{1a} and k_{1b} were determined, we calculated k_{2a} and k_{2b} from the relation $k_{2a}/k_{1a} = k_{2b}/k_{1b} = K^{-1}$ on assuming $\alpha_1 = \alpha_2$. As the total rate coefficient for reaction (1), $k_{1a} + k_{1b} = (1 - \alpha_1)\, k_1$, was reported to be (1.28–1.82) $\times 10^{-12}$ cm^3 molecule^{-1} s^{-1} for pressure up to 250 Torr of Ar,[14,24,26,29,31] we used the average value of $k_{1a} + k_{1b} = 1.5 \times 10^{-12}$ cm^3 molecule^{-1} s^{-1} in the fitting; this value fits satisfactorily with the experimental decay of CH_2I, when available, and the initial rise of CH_2OO in all experiments in SF_6 and those in N_2 and O_2 with $P \geq 60$ Torr. The yield of CH_2OO, $y = \alpha_2/(1 - \alpha_1) = [CH_2OO]_0/[CH_2I]_0$, implies that $k_{1a} = y\ (k_{1a} + k_{1b})$ and $k_{1b} = (1 - y)\ (k_{1a} + k_{1b})$; k_{1a} and k_{1b} could be determined from y and $k_{1a} + k_{1b}$. In the fit, the yield of CH_2OO was initially estimated with $y = [CH_2OO]_0/[CH_2I]_0$ in which $[CH_2OO]_0$ was estimated with a short extrapolation of the decay of $[CH_2OO]$ to $t = 0$ and $[CH_2I]_0 = -\Delta[CH_2I_2]$ when we assumed that all photolyzed CH_2I_2 produced $CH_2I + I$. Subsequent fine adjustments of y were performed on fitting the observed $[CH_2OO]$ profile; k_{1a} and k_{1b} were thereby derived.

The production of IO resulted mainly from two channels: reaction (2c) from $CH_2OO + I$ and reaction (5) from $ICH_2OO + I$. At low pressure, $[CH_2OO]$ is much greater than $[ICH_2OO]$, so that reaction (2c) is more important than reaction (5); in contrast, at high pressure, $[ICH_2OO]$ is much greater than $[CH_2OO]$, so that reaction (5) is more important than reaction (2c). Although the rate coefficient of k_{2c} was predicted to be 5.5×10^{-14} cm^3 molecule^{-1} s^{-1},[21] we found that we needed to set $k_{2c} = 9.0 \times 10^{-12}$ cm^3 molecule^{-1} s^{-1} to fit the rise of IO properly, especially at low pressures. This deviation of k_{2c} from a previous theoretical prediction is reasonable because this rate coefficient is sensitive to the barrier height and the calculated value of 7.9 kJ mol^{-1} might have been overestimated. From the sensitivity analysis shown in the supplementary material,[37] this rate coefficient has a negligible effect on the rate coefficient k_3 in fitting the profiles of CH_2OO.

It should be noted that the reaction

$$CH_2OO + CH_2I \rightarrow C_2H_4I + O_2(^3\Sigma_g^-) \tag{8}$$

with k_8 predicted to be 6.3×10^{-11} cm^3 molecule^{-1} s^{-1} (Ref. 21) is not included in the model because in our experiments O_2 was in excess so that most CH_2I was readily converted to CH_2OO or ICH_2OO. In experiments with significant $[CH_2I]$, this reaction has to be included in the model.

The fitting procedures thus became systematic on performing the following steps using either the Chemkin II program[41] or a fitting program written with MATLAB; the latter was more efficient and convenient to use; its validity was verified with the former. After the initial fitting of y with $k_{1a} + k_{1b}$ fixed to 1.5×10^{-12} cm^3 molecule^{-1} s^{-1} to derive k_{1a} and k_{1b}, and subsequently k_{2a} and k_{2b} using an initial guess of $K^{-1} = 70$, the rate coefficient of self-reaction of CH_2OO, k_3, was fitted with least squares to minimize the deviations of the simulated and observed temporal profiles of $[CH_2OO]$ and [IO]; k_{2c} and k_4–k_7 were fixed in the fitting. Values of k_4–k_6 were taken from the literature, as listed previously, but $k_7 = 1.5 \times 10^{-10}$ cm^3 molecule^{-1} s^{-1} had to be used to account for the decay of IO. The fit yielded $k_3 = (6.5 \pm 2.1) \times 10^{-11}$ cm^3 molecule^{-1} s^{-1}, but k_3 decreased with pressure for data in the pressure range 60–779 Torr. When K^{-1} was decreased to 40, we obtained $k_3 = (10.9 \pm 2.2) \times 10^{-11}$ cm^3 molecule^{-1} s^{-1}, with k_3 increasing with pressure for data in the pressure range 100–779 Torr.

We then varied the value of K systematically and repeated the fit, all data under varied experimental conditions were fitted satisfactorily to yield k_3 independent of pressure only when K^{-1} was in the range 50–60; the best fits were with $K^{-1} = 55$, which yields $k_3 = (8.2 \pm 1.4) \times 10^{-11}$ cm^3 molecule^{-1} s^{-1} for data in the pressure range 60–779 Torr. The value $K^{-1} = 55$ corresponds to $\Delta G = 9.8$ kJ mol^{-1} for reaction (1a), within expected uncertainties of the value 10.4 kJ mol^{-1} predicted with the CCSD(T)//B3LYP/aug-cc-pVTZ-pp method. Using this model, the simulated temporal profiles of CH_2I, CH_2OO, IO, ICH_2OO, I, and H_2CO for the experiment are shown with thick lines in Figs. 3 and 4; these simulated profiles of CH_2I, CH_2OO, and IO agree satisfactorily with experiments. In contrast, the profile simulated for IO in the experiment, shown as a dashed-dotted line (noted as "$k_{1c} = 0$") in Fig. 5 using this model, is significantly greater than the experimental data, to be discussed in Sec. IV B.

B. Decomposition of ICH_2OO^* or CH_2OO^* at P < 60 Torr

As indicated in Fig. 5, after fitting the profile of CH_2OO, the experimental temporal profile of IO disagrees with simulations using the mechanism discussed in Sec. IV A. The observed concentration of IO was significantly smaller than that simulated with this model and that of CH_2OO showed a rise less rapid than simulation. These deviations were observed for all experiments performed below 60 Torr.

As discussed in Sec. IV A, IO could be produced from two channels: $CH_2OO + I$ (reaction (2c)) and $ICH_2OO + I$ (reaction (5)). At low pressure, as $[ICH_2OO]$ is much smaller than $[CH_2OO]$, most IO was produced from $CH_2OO + I$. To reconcile the smaller [IO], we propose that some internally excited ICH_2OO^* or CH_2OO^* might have decomposed to form products other than CH_2OO or ICH_2OO at low pressure because of less efficient quenching. A similar mechanism

was also proposed by Eskola *et al.* for ICH_2OO^*.[29] Hence, for experiments below 60 Torr, we modified the original reaction (1a) to include two channels,

$$CH_2I + O_2 \rightarrow CH_2OO + I, \quad k_{1a}' = (1.5 \times 10^{-12} - k_{1b})\,\beta, \tag{1a'}$$

$$CH_2I + O_2 \rightarrow \text{products other than } CH_2OO \text{ or } ICH_2OO, \quad k_{1c} = (1.5 \times 10^{-12} - k_{1b})(1 - \beta) \tag{1c}$$

in which $k_{1c} = 0$ and the fraction of survival of CH_2OO $\beta = k_{1a}'/(k_{1a}' + k_{1c}) = 1$ for $P > 60$ Torr and β decreases with pressure for $P < 60$ Torr. The decomposition of some ICH_2OO^* or CH_2OO^* at low pressure consequently accounted for the smaller concentrations of CH_2OO and IO. The yield of CH_2OO is consequently revised to be $y = \beta\, k_{1a}/(k_{1a} + k_{1b})$ to include the data at low pressure; hence $k_{1a}' = (k_{1a} + k_{1b})\, y$, $k_{1b} = (k_{1a} + k_{1b})\,(1 - y/\beta)$, and $k_{1c} = (k_{1a} + k_{1b})\, y\,(1 - \beta)/\beta$. This decomposition channel at low pressure is further supported by our observation of infrared absorption bands of CO and CO_2 in the photolytic reaction of $CH_2I_2 + O_2$ at 248 nm for pressures below 40 Torr.

With this revised model, we adjusted β and y to fit the observed temporal profiles of IO and CH_2OO, with all other parameters determined the same way as in the case at high pressure. Subsequently, rate coefficient k_3 was fitted with least squares. After considering this decomposition channel, the temporal profiles of CH_2OO and IO were simulated satisfactorily, as shown in thick lines in Fig. 5 with $\beta = 0.78$ and 0.73 for experiment nos. 29 and 33, respectively. Twenty three experiments performed with total pressure below 60 Torr were fitted satisfactorily using this revised model with $\beta = 0.73$–0.92 or k_{1c} up to 3.9×10^{-13} cm^3 $molecule^{-1}$ s^{-1}, 26% of the total rate coefficient of reaction (1).

The less rapid rise of CH_2OO might be explained also by the decomposition mechanism. As at low pressure the quenching of ICH_2OO^* and CH_2OO^* is less facile, the proportion of the internally excited ICH_2OO^* or CH_2OO^* that decomposes increased, more at the earlier period of reaction. The proportion of the "loss" in CH_2OO was hence largest at the beginning and decreased at the later stage of reaction. When an efficient quencher SF_6 was employed, even at low pressure this delayed rise of CH_2OO disappeared, as indicated in Fig. S3 of the supplementary material.[37]

C. Fitted rate coefficients and their dependence on pressure

This fitting procedure worked well for 69 sets of data in total in the pressure range 7.6–779 Torr in which the pressure of O_2 was varied from 2.0 to 163.0 Torr, N_2 from 0 to 773.9 Torr, SF_6 from 0 to 62.7 Torr, and $[CH_2I]_0$ in the range (2.1–18.4) $\times$ 10^{13} molecule cm^{-3}. The experimental conditions, the fitted rate coefficients, and the values of y and β thus derived for some representative experiments are summarized in Table I; a complete list is available in Tables SI (N_2 and O_2) and SII (SF_6) of the supplementary material.[37]

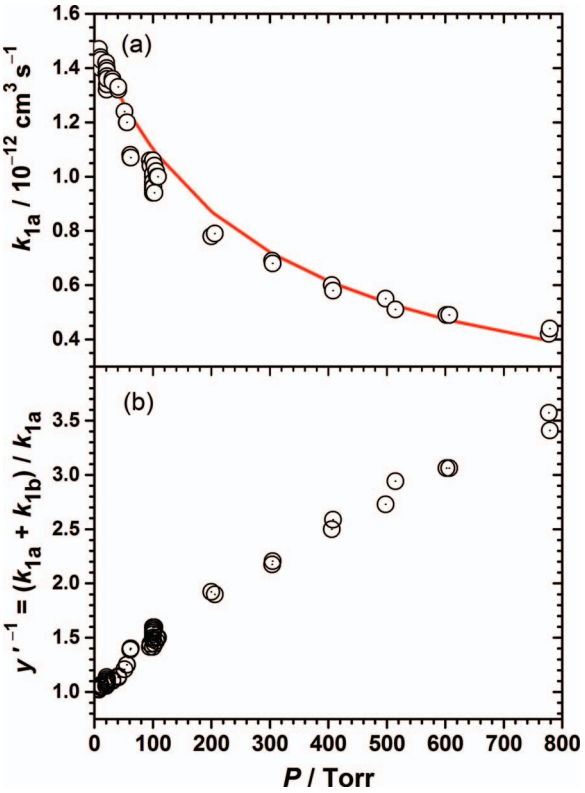

FIG. 6. Dependence on pressure of the rate coefficient for the formation of CH_2OO, k_{1a}. (a) k_{1a} as a function of total pressure P; the solid line is fitted according to Eq. (9); (b) $(k_{1a} + k_{1b})/k_{1a} = y'^{-1}$ as a function of P; $k_{1a} = k_{1a}' + k_{1c}$.

1. Pressure dependence of k_{1a} and k_{1b}

The pressure dependence of k_{1a} is shown in Fig. 6(a); k_{1a} represents the rate coefficient for the formation of CH_2OO from $CH_2I + O_2$. As expected, the rate coefficient decreases with pressure as the formation of ICH_2OO becomes more important. A plot of $(k_{1a} + k_{1b})/k_{1a}$ as a function of P is shown in Fig. 6(b); in this case k_{1a} takes into account the proportion that decomposes at low pressure. According to the rate expression shown in the supplementary material,[37]

$$\frac{k_{1a} + k_{1b}}{k_{1a}} = 1 + \frac{k_q[\mathrm{M}]}{k_{-2}}. \tag{9}$$

The linear relation between $(k_{1a} + k_{1b})/ k_{1a}$ and [M] $(=P)$ and an intercept $\sim$1 are satisfactorily demonstrated in Fig. 6(b), supporting the validity of our model. Using this equation, we were able to derive $k_q/k_{-2} = (1.1 \pm 0.1) \times 10^{-19}$ cm^3 $molecule^{-1}$.

The dependence of k_{1b} on pressure is shown in Fig. 7(a); k_{1b} represents the rate coefficient for the formation of ICH_2OO from $CH_2I + O_2$. A linear rise with pressure is observed for k_{1b} at low pressure; k_{1b} levels off at high pressure, characteristic of quenching stabilization of ICH_2OO. A plot of $(k_{1a} + k_{1b})/k_{1b}$ as a function of P^{-1} is shown Fig. 7(b); because this channel is important only at high pressure, we plot data only with $P \geq 100$ Torr. According to the rate

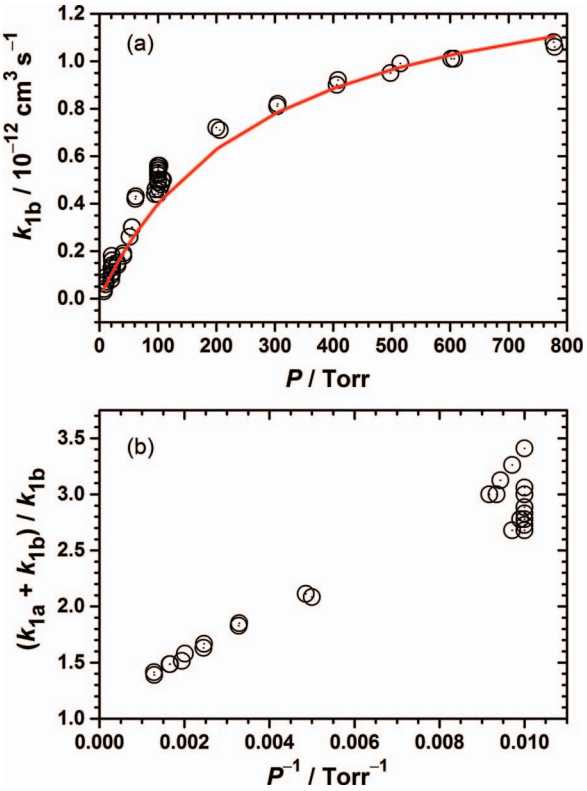

FIG. 7. Dependence on pressure of the rate coefficient for the formation of ICH_2OO, k_{1b}. (a) k_{1b} as a function of total pressure P; the solid line is fitted according to $k_{1b} = 1.5 \times 10^{-12}$ cm^3 molecule^{-1} s^{-1} $- k_{1a}$; (b) $(k_{1a} + k_{1b})/k_{1b}$ as a function of P^{-1}, $P > 100$ Torr.

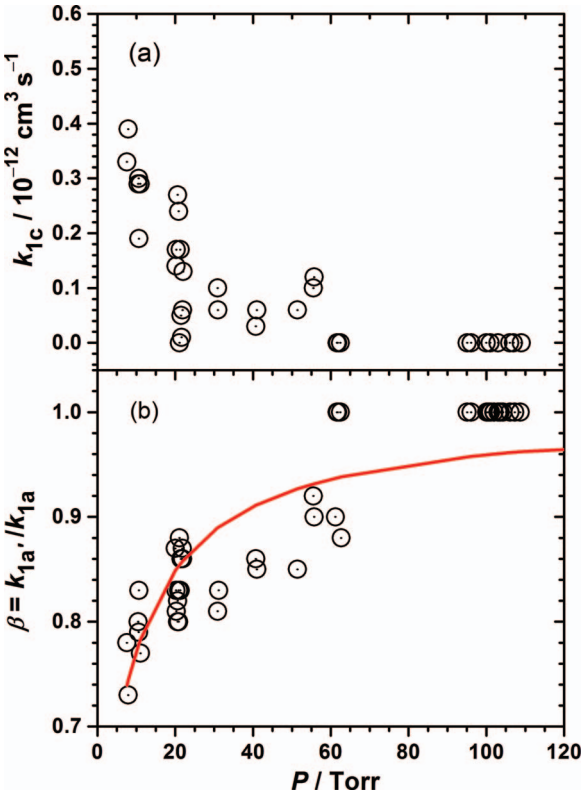

FIG. 8. Dependence on total pressure of k_{1c} (a) and the fraction of survival of CH_2OO, β, in the pressure range 7–100 Torr (b); the solid line is fitted according to Eq. (11).

expression shown in the supplementary material,[37]

$$\frac{k_{1a} + k_{1b}}{k_{1b}} = 1 + \frac{k_{-2}}{k_q[\mathrm{M}]}. \tag{10}$$

The linear relation between $(k_{1a} + k_{1b})/k_{1b}$ and P^{-1} and an intercept ~1 are satisfactorily demonstrated in Fig. 7(b). The satisfactory dependence of both k_{1a} and k_{1b} over a broad pressure range indicates that our model is adequate to describe the variation of concentration of CH_2OO and IO. However, because we assumed that $k_{1a} + k_{1b} = 1.5 \times 10^{-12}$ cm^3 molecule^{-1} s^{-1}, the equation $k_{1b} = 1.5 \times 10^{-12}$ cm^3 molecule^{-1} s^{-1} $- k_{1a}$ instead of Eq. (10) should be used for derivation of k_{1b}.

Because of the equilibrium relationship, $K^{-1} = k_{2a}/k_{1a} = \alpha_1 k_{2b}/\alpha_2 k_{1b} = 55$, the pressure dependence of k_{2a} and k_{2b} follows that of k_{1a} and k_{1b}, respectively.

2. Pressure dependence of k_{1c}

The dependence of k_{1c} on pressure is shown in Fig. 8(a) and the dependence of β, the fraction of survived CH_2OO, on pressure is shown in Fig. 8(b); because of the smaller values, the errors in these measurements are greater than others. An initial increase in β with pressure before leveling off, similar to that of k_{1b}, was observed; this is characteristic of quenching stabilization. A decrease with pressure is observed for k_{1c}; the value becomes negligible near 60 Torr. The observed pressure dependence is consistent with a mechanism of stabilization of ICH_2OO^* and CH_2OO^* by collisional quenching. The β values are fitted to an equation

$$\beta = 1 - (0.47 \pm 0.11)/[1 + (3.2 \pm 1.2) \times 10^{-18}\,[\mathrm{M}]]. \tag{11}$$

Because of the large uncertainties in β, the fitting reproduce β values to only within 0.08.

3. Determination of k_3

The fitted rate coefficient for self-reaction of CH_2OO, k_3, ranged from 5.6 to 12.0 $\times 10^{-11}$ cm^3 molecule^{-1} s^{-1}, with an average of all data $k_3 = (8.2 \pm 1.4) \times 10^{-11}$ cm^3 molecule^{-1} s^{-1} for experiments in N_2 and O_2; the error limits represent one standard deviation in averaging. Some representative sensitivity analyses are shown in the supplementary material.[37] At high pressure, the analysis clearly shows that reactions (1a), (1b) and (2b) are more sensitive to the variation of $[CH_2OO]$ than reaction (3), but the factors of reactions (1a) and (1b) have similar values with opposite signs because these reactions are competing with CH_2I for the formation of either CH_2OO or ICH_2OO. The sensitivity of reaction (3), $\partial x/\partial(\ln k_3)$, in which x is the mass fraction of CH_2OO, indicates that k_3 has greater errors at high pressure than at low pressure, mainly because $[CH_2OO]$ is small relative to $[ICH_2OO]$. At lower pressure $[CH_2OO]$ is much greater than $[ICH_2OO]$ and the sensitivity of reaction (3) is greater than of reactions (2a) and (2b), but still smaller than of reactions (1a) and (1b). However, the effect of reactions (1a) and (1b) on k_3 cancels each other. Even under such conditions and in the critical range 20–150 μs, $\partial(\ln k_3)/\partial(\ln k_i)$

$\cong$ 0.4–1.0 for i = 2a and 2b, indicating that k_3 is sensitive to values of k_{2a} and k_{2b}. Considering the large variations in k_{2a} and k_{2b} under our experimental conditions, the consistency of values of k_3 throughout the pressure range supports the validity of the mechanism including decomposition reaction (1c).

Two assumptions were made in these fits: $k_{1a} + k_{1b} = 1.5 \times 10^{-12}$ cm^3 molecule^{-1} s^{-1} and $\alpha_1/\alpha_2 = 1$. The former was actually tested with our experimental data, even at high pressure, and we fixed this value simply to minimize the variables in our fitting. The value of α_1/α_2 might deviate slightly from 1; a deviation of 30% implies a deviation of k_{2b} by 30%, which translates to ~20% in k_3 at low pressure. Considering the estimated relative error of 20% in concentration measurements of CH_2OO, which translates to ~60% error in k_3 at high pressure and ~30% at low pressure based on sensitivity analysis, 24% error induced by the uncertainty of K^{-1} (=55 ± 15), 17% error in the least-square fit of each individual temporal profile, we report $k_3 = (8 \pm 4) \times 10^{-11}$ cm^3 molecule^{-1} s^{-1} with the error representing the 95% confidence level.

Previously, using IR absorption to monitor CH_2OO, we could only roughly estimate the rate coefficient of k_3 because of large uncertainties.[21] Because the IR probe beam did not follow the UV photolysis beam, the average concentration in the photolysis volume hence differed from that of the IR-probed volume. The conversion between concentrations of CH_2OO in the UV-photolyzed volume and the IR-probed volume had large errors. The initial concentration of CH_2I in the photolyzed volume was estimated with the UV absorption cross section of CH_2I_2 and the laser fluence, which was estimated from the energy and the size of the laser beam. The concentration of CH_2OO measured from IR absorption also had large errors because the IR absorption cross section predicted with quantum-chemical computations might have large errors which affect the bimolecular rate coefficient by approximately the same factor. Furthermore, the mechanism employed previously ignored reactions (1b) and (1c), and also employed theoretically predicted rate coefficients for reactions (2a)–(2c). All these factors might result to an underestimated error bar of our previous estimate. The dependence of k_3 on temperature is expected to be small, so the previously reported value of $k_3 = (4 \pm 2) \times 10^{-10}$ cm^3 molecule^{-1} s^{-1} at 343 K might have been overestimated. Our determination of $k_3 = (8 \pm 4) \times 10^{-11}$ cm^3 molecule^{-1} s^{-1} at 295 K in this work agrees with the recently reported value $k_3 = (6.0 \pm 2.1) \times 10^{-11}$ cm^3 molecule^{-1} s^{-1} at 297 K by Buras *et al.*,[32] even though a simplified mechanism was employed in that work.

D. Yield of CH_2OO and its dependence on pressure

In Fig. 9 we plot the reciprocal yield of CH_2OO, $y^{-1} = (k_{1a}' + k_{1b} + k_{1c})/k_{1a}' = (k_{1a} + k_{1b})/k_{1a}'$, as a function of total density [M] for the pressure range 7.6–779.2 Torr. These data were fitted with the equations

$$y^{-1} = (1.24 \pm 0.03) + (9.13 \pm 0.33) \times 10^{-20}\,[\mathrm{M}], \quad \mathrm{M} = \mathrm{O_2}\ \mathrm{or}\ \mathrm{N_2} \tag{12}$$

in which [M] is the density in molecule cm^{-3}; the errors represent one standard deviation in fitting. Our data are compared with previous reports in Fig. 9. The smaller yield of CH_2OO (greater y^{-1}) at low pressure is due to the decomposition of CH_2OO^*/ICH_2OO^*; this reduction of yield would not appear in the experiments with I-atom detection. It is unclear why Huang *et al.* observed significantly different pressure dependence on N_2 and O_2;[30] our results for M = O_2 and N_2 agree satisfactorily with their report for M = He [slope = (0.93 ± 0.13) × 10^{-19}] and O_2 [slope = (1.1 ± 0.1) × 10^{-19}], but are much smaller than for M = N_2 [slope = (2.4 ± 0.4) × 10^{-19}].[30] Our results also have a pressure dependence much less than that reported by Stone *et al.*[31] with M = N_2 and O_2 [slope = (1.90 ± 0.11) × 10^{-19} for all data].

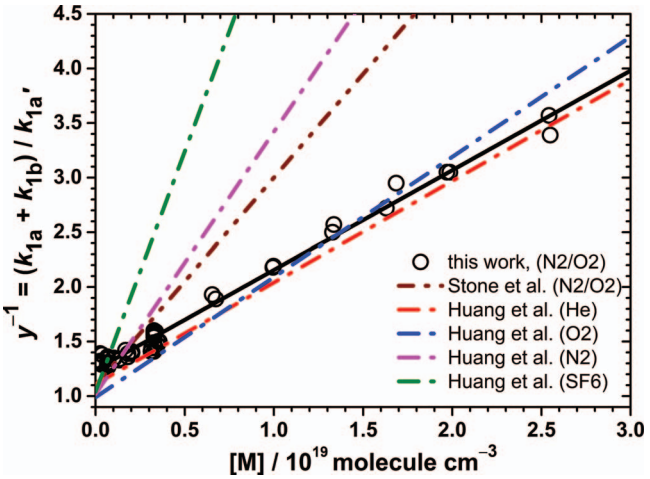

FIG. 9. Reciprocal initial yield y of CH_2OO from $CH_2I + O_2$ as a function of total density [M]. $y^{-1} = (k_{1a} + k_{1b})/k_{1a}' = (k_{1a} + k_{1b})/\beta k_{1a}$. The data were fitted to a line with intercept 1.24 and slope 9.1 × 10^{-20} cm^3 molecule^{-1} for M = O_2 or N_2. The results of Huang *et al.*[30] for M = He, O_2, and N_2, with slopes 0.95, 1.14, and 2.41 × 10^{-19} cm^3 molecule^{-1}, respectively, and the result of Stone *et al.*[31] for M = O_2 or N_2, with a slope 1.90 × 10^{-19} cm^3 molecule^{-1}, are also shown for comparison.

Our assumption of $-\Delta[CH_2I_2] = [CH_2I]_0$ might overestimate $[CH_2I]_0$ by as much as 15%, but not significantly enough to explain the discrepancies. When we tested the power dependence of this discrepancy, we found that this discrepancy was not due to secondary photolysis of CH_2I; it is likely due to the error of the reported cross section of CH_2I. Some uncertainties in these previous reports might have resulted from the indirect methods employed by observation of I atoms and H_2CO rather than CH_2OO, and the uncertainties in analysis of observed temporal profiles with their models. It should be noted that we performed experiments at 248 nm whereas Huang *et al.* employed light at 355 nm.[30] Weather the difference in internal energy of CH_2I affects the stabilization of ICH_2OO, even at high pressures, requires further investigation. However, from the results of Stone *et al.* in which laser light at both 248 nm and 355 nm was used, the effect of photolysis wavelength on yield of CH_2OO is insignificant.[31]

The estimated yields of CH_2OO from $CH_2I + O_2$ at 298 K and 760 Torr in air, ~15% reported by Huang *et al.*[30] and 18% by Stone *et al.*,[31] were proposed to have significant implications for the oxidation chemistry of halogen-containing organic compounds and for the atmospheric chemistry in marine regions with large concentrations of CH_2I_2.

TABLE II. Summary of the rate coefficients and yield of CH_2OO derived from the $CH_2I + O_2$ system at 295 K.

	Reaction/description	Expression[a]	Conditions	Assumptions[a]
k_{1a}	$CH_2I + O_2 \rightarrow CH_2OO + I$	1.5×10^{-12} /{1 + (1.1 ± 0.1) × 10^{-19} [M]}	P ≥ 60 Torr	$k_{1a} + k_{1b} = 1.5 \times 10^{-12}$
k_{1a}'	$CH_2I + O_2 \rightarrow CH_2OO + I$	$\beta \times 1.5 \times 10^{-12}$ /{1 + (1.1 ± 0.1) × 10^{-19} [M]}	P < 60 Torr	$k_{1a}' + k_{1b} + k_{1c} = 1.5 \times 10^{-12}$
β	Fraction of survival of CH_2OO at low P, $\beta = k_{1a}'/k_{1a}$	$1 - (0.47 \pm 0.11)/\{1 + (3.2 \pm 1.2) \times 10^{-18}$ [M]}[b]	P < 60 Torr	
k_{1b}	$CH_2I + O_2 \xrightarrow{M} ICH_2OO$	$1.5 \times 10^{-12} - k_{1a}$		$k_{1a} + k_{1b} = 1.5 \times 10^{-12}$
k_{1c}	$CH_2I + O_2 \rightarrow$ products other than CH_2OO or ICH_2OO	$k_{1a}\ (1-\beta)$	P < 60 Torr	
k_{2a}	$CH_2OO + I \rightarrow CH_2I + O_2$	$55\ k_{1a}$		$K^{-1} = 55$
k_{2b}	$CH_2OO + I \xrightarrow{M} ICH_2OO$	$55\ k_{1b}$		$K^{-1} = 55$, $\alpha_1 = \alpha_2$
k_{2c}	$CH_2OO + I \rightarrow H_2CO + IO$	9.0×10^{-12}		P-independent
k_3	$CH_2OO + CH_2OO \rightarrow 2\ H_2CO + O_2\ (^1\Delta_g)$	$(8 \pm 4) \times 10^{-11}$		P-independent
y	Yield of CH_2OO, $y^{-1} = (k_{1a}' + k_{1b} + k_{1c})/k_{1a}' = (k_{1a} + k_{1b})/k_{1a}'$	$y^{-1} = (1.24 \pm 0.03) + (9.13 \pm 0.33) \times 10^{-20}$ [M], M = O_2 or N_2		$-\Delta[CH_2I_2] = [CH_2I]_0$

[a]Rate coefficient in cm^3 $molecule^{-1}$ s^{-1}, [M] in molecule cm^{-3}, and K, β, and y are dimensionless. K is the equilibrium constant of the reaction $CH_2I + O_2 = CH_2OO + I$; $K^{-1} = 55$ provides the best fitting.

[b]Approximate fitting of the scattered data below 60 Torr.

Our estimate of a yield ~30% at 295 K and 760 Torr would enhance these effects significantly.

Following the same method[21] to simulate the experimental conditions in the laboratory investigations of the ozonolysis of C_2H_4 using the revised k_3 value and a model reported previously,[9] we found that, when the self-reaction of CH_2OO is included in the model, the simulated yield of hydroperoxymethyl formate [HPMF, CH_2(OOH)–O–CHO] and formic acid anhydride [FA, $(HCO)_2O$] decreased by ~7% and that of HCOOH increased by ~3%. The H_2CO produced due to the self-reaction of CH_2OO accounts for an additional yield ~0.03. When we increased the rate coefficient for O_3 + alkene from 1×10^{-18} cm^3 $molecule^{-1}$ s^{-1} for C_2H_4 to 1×10^{-16} cm^3 $molecule^{-1}$ s^{-1} for larger alkenes,[30] the simulated yield of compounds due to the reaction of Criegee intermediate + HCOOH, corresponding to HPMF + FA in O_3 + C_2H_4, decreased by 25%–30%, whereas that of HCOOH increased by 10%–12%. Furthermore, the additional carbonyl compounds produced from the self-reaction of the Criegee intermediates account for a yield 0.11–0.14, explaining the observed stoichiometry ratio larger than unity. Even though the significantly reduced value of the rate coefficient k_3 decreased its effect on the laboratory ozonolysis experiments, it might play an important role when the concentration of CH_2OO is large.

The rate coefficients k_{1a}, k_{1a}', k_{1b}, k_{1c}, k_{2a}, k_{2b}, k_{2c}, k_3, and values of β (fraction of survival of CH_2OO) and y (yield of CH_2OO) derived in this work are summarized in Table II.

V. CONCLUSION

To investigate the detailed kinetics of the $CH_2I + O_2$ reaction, we monitored the UV absorption of CH_2I_2, CH_2I, IO, and CH_2OO simultaneously in the reaction system of $CH_2I + O_2$ at 295 K upon photolysis of a flowing mixture of CH_2I_2, O_2, and N_2 (or SF_6) at 248 nm. Using a detailed mechanism for the reaction, we simulated the temporal profiles of CH_2OO and IO that agreed satisfactorily with experimental data over a wide range of experimental conditions with P = 7.6–779 Torr. We found that, at pressure below 60 Torr, some internally excited ICH_2OO^* or CH_2OO^* decomposed; the fraction of survival $\beta = k_{1a}'/(k_{1a}' + k_{1c})$ was determined to be as small as ~0.75 near 7.8 Torr.

The feature of our mechanism is that we clearly specified three channels for the reaction $CH_2I + O_2$ and three channels for $CH_2OO + I$, and include the self-reaction of CH_2OO that becomes important when the concentration of CH_2OO is large. The dependence of derived rate coefficients on pressure for the formation of $CH_2OO + I$ (k_{1a}), ICH_2OO (k_{1b}), and other products (k_{1c}) from $CH_2I + O_2$ and the formation of $CH_2I + O_2$ (k_{2a}), ICH_2OO (k_{2b}), and H_2CO + IO (k_{2c}) from $CH_2OO + I$ was determined; they conform to the expected behavior for enhanced stabilization of ICH_2OO at higher pressure. We also determined a rate coefficient k_3 = (8 ± 4) × 10^{-11} cm^3 $molecule^{-1}$ s^{-1} for the self-reaction of CH_2OO, significantly smaller than our previous estimate at 343 K using IR absorption.

The dependence on pressure of the yield y of CH_2OO from $CH_2I + O_2$ conforms to the equation y^{-1} = (1.24 ± 0.03) + (9.13 ± 0.33) × 10^{-20} [M] in which [M] = O_2 or N_2 is the total density in molecule cm^{-3}. This dependence on pressure is smaller than in previous reports; the ~30% yield of CH_2OO at 760 Torr much greater than values 15%–18% in previous reports might have a significant impact on the atmospheric chemistry of marine regions.

ACKNOWLEDGMENTS

Ministry of Science and Technology, Taiwan (Grant Nos. NSC102-2745-M009-001-ASP and NSC100-2113-M-001-008-MY3) and the Ministry of Education, Taiwan ("ATU Plan" of National Chiao Tung University) supported this work. The National Center for High-Performance Computing provided computer time.

[1]D. Johnson and G. Marston, Chem. Soc. Rev. **37**, 699 (2008).
[2]J. G. Calvert, R. Atkinson, J. A. Kerr, S. Madronich, G. K. Moortgat, T. J. Wallington, and G. Yarwood, *The Mechanisms of Atmospheric Oxidation of the Alkenes* (Oxford University Press, Oxford, UK, 2000), pp. 172–335.

[3]O. Horie and G. K. Moortgat, Acc. Chem. Res. **31**, 387 (1998).
[4]R. Criegee and G. Wenner, Justus Liebigs Ann. Chem. **564**, 9 (1949).
[5]W. Sander, Angew. Chem. Int. Ed. Engl. **29**, 344 (1990).
[6]W. H. Bunnelle, Chem. Rev. **91**, 335 (1991).
[7]S. Hatakeyama and H. Akimoto, Res. Chem. Intermed. **20**, 503 (1994).
[8]G. Marston, Science **335**, 178 (2012).
[9]P. Neeb, O. Horie, and G. K. Moortgat, J. Phys. Chem. A **102**, 6778 (1998).
[10]C. A. Taatjes, D. E. Shallcross, and C. J. Percival, Phys. Chem. Chem. Phys. **16**, 1704 (2014).
[11]C. A. Taatjes, G. Meloni, T. M. Selby, A. J. Trevitt, D. L. Osborn, C. J. Percival, and D. E. Shallcross, J. Am. Chem. Soc. **130**, 11883 (2008).
[12]O. Welz, J. D. Savee, D. L. Osborn, S. S. Vasu, C. J. Percival, D. E. Shallcross, and C. A. Taatjes, Science **335**, 204 (2012).
[13]J. M. Beames, F. Liu, L. Lu, and M. I. Lester, J. Am. Chem. Soc. **134**, 20045 (2012).
[14]L. Sheps, J. Phys. Chem. Lett. **4**, 4201 (2013).
[15]W.-L. Ting, Y.-H. Chen, W. Chao, M. C. Smith, and J. J. Lin, Phys. Chem. Chem. Phys. **16**, 10438 (2014).
[16]Y.-T. Su, Y.-H. Huang, H. A. Witek, and Y.-P. Lee, Science **340**, 174 (2013).
[17]M. Nakajima and Y. Endo, J. Chem. Phys. **139**, 101103 (2013).
[18]M. C. McCarthy, L. Cheng, K. N. Crabtree, O. Martinez, T. L. Nguyen, C. C. Womack, and J. F. Stanton, J. Phys. Chem. Lett. **4**, 4133 (2013).
[19]C. A. Taatjes, O. Welz, A. J. Eskola, J. D. Savee, D. L. Osborn, E. P. F. Lee, J. M. Dyke, D. W. K. Mok, D. E. Shallcross, and C. J. Percival, Phys. Chem. Chem. Phys. **14**, 10391 (2012).
[20]D. Stone, M. Blitz, L. Daubney, N. U. M. Howes, and P. Seakins, Phys. Chem. Chem. Phys. **16**, 1139 (2014).
[21]Y.-T. Su, H.-Y. Lin, R. Putikam, H. Matsui, M. C. Lin, and Y.-P. Lee, Nat. Chem. **6**, 477 (2014).
[22]Y. Liu, K. D. Bayes, and S. P. Sander, J. Phys. Chem. A **118**, 741 (2014).
[23]J. Sehested, T. Ellermann, and O. J. Nielsen, Int. J. Chem. Kinet. **26**, 259 (1994).
[24]A. Masaki, S. Tsunashima, and N. Washida, J. Phys. Chem. **99**, 13126 (1995).
[25]S. Enami, J. Ueda, M. Goto, Y. Nakano, S. Aloisio, S. Hashimoto, and M. Kawasaki, J. Phys. Chem. A **108**, 6347 (2004).
[26]S. Enami, Y. Sakamoto, T. Yamanaka, S. Hashimoto, M. Kawasaki, K. Tonokura, and H. Tachikawa, Bull. Chem. Soc. Jpn. **81**, 1250 (2008).
[27]T. Gravestock, M. Blitz, W. Bloss, and D. E. Heard, ChemPhysChem **11**, 3928 (2010).
[28]V. G. Stefanopoulos, V. C. Papadimitriou, Y. G. Lazarou, and P. Papagiannakopoulos, J. Phys. Chem. A **112**, 1526 (2008).
[29]A. J. Eskola, D. Wojcik-Pastuszka, E. Ratajczak, and R. S. Timonen, Phys. Chem. Chem. Phys. **8**, 1416 (2006).
[30]H. Huang, A. Eskola, and C. A. Taatjes, J. Phys. Chem. Lett. **3**, 3399 (2012); **4**, 3824 (2013).
[31]D. Stone, M. Blitz, L. Daubney, T. Ingham, and P. Seakins, Phys. Chem. Chem. Phys. **15**, 19119 (2013).
[32]Z. J. Buras, R. M. I. Elasmra, and W. H. Green, J. Phys. Chem. Lett. **5**, 2224 (2014).
[33]M.-N. Su and J. J. Lin, Rev. Sci. Instrum. **84**, 086106 (2013).
[34]M.-N. Su and J. J. Lin, GSTF J. Chem. Sci. (JChem) **1**, 52 (2013).
[35]S. P. Sander, J. Abbatt, J. R. Barker, J. B. Burkholder, R. R. Friedl, D. M. Golden, R. E. Huie, C. E. Kolb, M. J. Kurylo, G. K. Moortgat, V. L. Orkin, and P. H. Wine, "Chemical kinetics and photochemical data for use in atmospheric studies," Evaluation Number 17, JPL Publication 10-6, Jet Propulsion Laboratory, Pasadena, 2011, see http://jpldataeval.jpl.nasa.gov.
[36]E. P. F. Lee, D. K. W. Kok, D. E. Shallcross, C. J. Percival, D. L. Osborn, C. A. Taayjes, and J. M. Dyke, Chem. Eur. J. **18**, 12411 (2012).
[37]See supplementary material at http://dx.doi.org/10.1063/1.4894405 for analysis of the transient absorption spectra, kinetic analysis, additional temporal profiles, a complete list of experimental conditions and fitted results, and sensitivity analysis.
[38]H. Y. Chen, C.-Y. Lien, W.-Y. Lin, Y. T. Lee, and J. J. Lin, Science **324**, 781 (2009).
[39]Z. J. Buras, R. M. I. Elasamra, A. Jalan, J. E. Middaugh, and W. H. Green, J. Phys. Chem. A **118**, 1997 (2014).
[40]R. Atkinson, D. L. Baulch, R. A. Cox, J. N. Crowley, R. F. Hampson, R. G. Hynes, M. E. Jenkin, M. J. Rossi, and J. Troe, Atmos. Chem. Phys. **7**, 981 (2007).
[41]R. J. Kee, F. M. Rupley, and J. A. Miller, Chemkin-II, "A Fortran chemical kinetics package for the analysis of gas-phase chemical kinetics," Sandia Report, SAND89-8009B, 1995.